Cellular and Molecular Life Sciences (2023) 80:301
https://doi.org/10.1007/s00018-023-04958-7

ORIGINAL ARTICLE

FKBP5 deficiency attenuates calcium oxalate kidney stone formation by suppressing cell–crystal adhesion, apoptosis and macrophage M1 polarization via inhibition of NF-κB signaling

Qianlin Song[1,2] · Chao Song[1] · Xin Chen[2,3] · Yunhe Xiong[1] · Lijun Li[4] · Wenbiao Liao[1] · Longjian Xue[4] · Sixing Yang[1]

Received: 12 July 2023 / Revised: 7 September 2023 / Accepted: 8 September 2023 / Published online: 23 September 2023

Abstract

Surgical crushing of stones alone has not addressed the increasing prevalence of kidney stones. A promising strategy is to tackle the kidney damage and crystal aggregation inherent in kidney stones with the appropriate therapeutic target. FKBP prolyl isomerase 5 (FKBP5) is a potential predictor of kidney injury, but its status in calcium oxalate (CaOx) kidney stones is not clear. This study attempted to elucidate the role and mechanism of FKBP5 in CaOx kidney stones. Lentivirus and adeno-associated virus were used to control FKBP5 expression in a CaOx kidney stone model. Transcriptomic sequencing and immunological assays were used to analyze the mechanism of FKBP5 deficiency in CaOx kidney stones. The results showed that FKBP5 deficiency reduced renal tubular epithelial cells (RTEC) apoptosis and promoted cell proliferation by downregulating BOK expression. It also attenuated cell–crystal adhesion by downregulating the expression of CDH4. In addition, it inhibited M1 polarization and chemotaxis of macrophages by suppressing CXCL10 expression in RTEC. Moreover, the above therapeutic effects were exerted by inhibiting the activation of NF-κB signaling. Finally, in vivo experiments showed that FKBP5 deficiency attenuated stone aggregation and kidney injury in mice. In conclusion, this study reveals that FKBP5 deficiency attenuates cell–crystal adhesion, reduces apoptosis, promotes cell proliferation, and inhibits macrophage M1 polarization and chemotaxis by inhibiting NF-κB signaling. This provides a potential therapeutic target for CaOx kidney stones.

Keywords Kidney stones · FKBP5 · NF-κB signaling · Cell–crystal adhesion · Immune regulation

Introduction

The prevalence and recurrence rates of kidney stones, which represent a chronic kidney disease, are astounding. In China, the prevalence of kidney stones is 6.5% in men and 5.1% in women [1]. In the United States, the prevalence is 10.9%

Qianlin Song, Chao Song and Xin Chen contributed equally to this work and shared the first authorship.

✉ Xin Chen
drxinchen@whu.edu.cn

✉ Longjian Xue
xuelongjian@whu.edu.cn

✉ Sixing Yang
sxyang@whu.edu.cn

[1] Department of Urology, Renmin Hospital of Wuhan University, Jiefang Road 238, Wuhan 430060, Hubei, People's Republic of China

[2] Central Laboratory, Renmin Hospital of Wuhan University, Jiefang Road 238, Wuhan 430060, Hubei, People's Republic of China

[3] Reproductive Medical Center, Renmin Hospital of Wuhan University and Hubei Clinic Research Center for Assisted Reproductive Technology and Embryonic Development, Jiefang Road 238, Wuhan 430060, Hubei, People's Republic of China

[4] School of Power and Mechanical Engineering, The Institute of Technological Science, Wuhan University, South Donghu Road 8, Wuhan 430072, Hubei, People's Republic of China

in men and 9.5% in women [2]. The recurrence rate of kidney stones is as high as 50% within 5 years. Moreover, the prevalence of kidney stones continues to increase [3]. The prolonged course of kidney stones can lead to the evolution of irreversible chronic kidney disease due to renal fibrosis and inflammation of the renal parenchyma [4]. Therefore, surgical crushing and stone removal are inadequate for managing kidney stones. We need to seek precise and effective drug targets to stop the progression of kidney damage and inflammation inherent in kidney stones.

FKBP5 is a member of the family of FK506-binding immunophilins (FKBPs) [5]. FKBP5 is usually upregulated in response to stimuli such as stress, aging, and glucocorticoids [6, 7]. FKBP5 is thought to be associated with acute or chronic kidney injury and may reflect the pathological state of tubulointerstitial inflammation and fibrosis in diabetic nephropathy [5, 8]. However, the status and role of FKBP5 in kidney stones have yet to be reported.

The NF-κB signaling pathway is a classic proinflammatory signaling pathway that has essential regulatory roles in cell adhesion, apoptosis, and the immune response [9]. It has been reported that FKBP5 is a robust regulator of NF-κB signaling [10, 11]. In addition, activation of NF-κB signaling is involved in developing kidney stones [12]. Therefore, we hypothesized that FKBP5 might regulate inflammation and injury in CaOx kidney stones through NF-κB signaling, which is involved in the progression of CaOx kidney stones.

In this study, we investigated the mechanism of the FKBP5/NF-κB signaling axis in CaOx kidney stones to provide potential therapeutic targets for CaOx kidney stones.

Materials and methods

Animal experiments

The animal experiments in this study were approved by the Animal Ethics Committee of the Renmin Hospital of Wuhan University (Issue No. 20221008A). All C57BL/6 male mice (8 weeks old) were fed standard food and water. All subgroups in the animal experiments consisted of 8 mice each. Experimental grouping was performed as follows:

Saline group: A volume of 100 µl of saline was injected intraperitoneally daily for 6 days.

Glyoxylate (Gly) group: Established according to a previous study [13]. 100 µl of Gly (80 mg/kg) (HY-79494, MedChemExpress, Wuhan, China) was injected intraperitoneally daily for 6 days.

Saline + AAV-sh-*FKBP5* group: the shRNA-*FKBP5* targeting mouse FKBP5 was packaged into the adeno-associated virus (AAV) serotype 9 vector by WZ Biosciences Inc. (Jinan, China). C57BL/6 male mice (4 weeks old) were used to construct *FKBP5* deficient mice. The mice were anesthetized to expose the kidney, the ureter was blocked using a hemostatic clip, and then AAV containing sh-*FKBP5* (50 µl, 5×10^{10} vg) was injected into the renal pelvis. The expression of FKBP5 was measured after 4 weeks. Then, the mice received a daily intraperitoneal injection of 100 µl of saline for 6 days.

Saline + AAV-NC group: Similar to the Saline + AAV-sh-*FKBP5* group except that, the difference is that the AAV containing sh-*FKBP5* was replaced with an AAV containing an empty vector.

Gly + AAV-sh-*FKBP5* group: Similar to the Saline + AAV-sh-*FKBP5* group except that the saline received for 6 days was replaced with Gly.

Gly + AAV-NC group: Similar to the Saline + AAV-NC group except that the saline received for 6 days was replaced with Gly.

On the 6th day, urine was collected from the mice through metabolic cages. Blood was collected from the retro-orbital plexus and centrifuged, and serum was obtained. Finally, mice were euthanized by overdose of isoflurane, and kidneys were collected for subsequent experiments.

Cell culture

Human kidney proximal tubule cells (HK-2) and human leukemia monocytic cells (THP-1) were purchased from China Center for Type Culture Collection (Wuhan, China), and human embryonic kidney cells (HKE-293) were purchased from Basic Medical Sciences Chinese Academy of Medical Sciences (Beijing, China). HK-2 cells, THP-1 cells, and HEK-293 cells were cultured using Dulbecco's modified Eagle's medium/nutrient mixture F-12 medium, Roswell Park Memorial Institute 1640 medium, and minimum essential medium, respectively. All cells were incubated in a standard incubator with conventional 5% CO_2 at 37 °C.

Cellular grouping and intervention

It is well known that oxalate (Ox) is a significant component of approximately 80% of kidney stones [14]. In addition, HEK-293 cells are often studied in research on kidney stones in vitro [15, 16]. Therefore, in vitro, CaOx kidney stone models were constructed using 1 mmol/l Ox (75688, Sigma, USA) intervention in HK-2 cells and HEK-293 cells.

Gene control: Lentiviral vectors for *FKBP5* overexpression and knockdown and viral negative control, plasmids for *BOK* and *CDH4* overexpression and negative control, and plasmids for *JAK2* knockdown and negative control were purchased from WZ Biosciences Inc. According to the manufacturer's instructions, the above genetic tools were introduced into HK-2 cells and HEK-293 cells. Briefly, the lentiviral vector was introduced into the cells with transfection reagent, and the stably transfected cell lines were then

screened using 5 μg/ml of puromycin. Plasmids were added to the cells after mixing with Lipo2000 (11668019, Thermo Fisher Scientific Inc., USA) in basal medium for 20 min, and plasmid incubation was conducted together with other interventions after 24 h.

M0 macrophage differentiation: When the density of THP-1 cells reached 70–80%, medium containing 100 ng/ml of phorbol-12-myristate-13-acetate (PMA) (P8139, Sigma) was added, and the cells were incubated for 24 h.

Von Kossa staining

Von Kossa staining was used to detect the extent of stone aggregation in the kidneys of mice. In brief, wax blocks of kidney samples were sectioned, dewaxed, and washed. They sections were placed in silver nitrate staining solution under ultraviolet light for 10 min, washed, restained, and sealed. Finally, they were observed and recorded under a microscope.

Immunohistochemistry

Kidney tissues were sectioned and dewaxed; washed three times with distilled water, subjected to antigen repair and blocking processes; incubated for 12 h at 4 °C with primary antibodies (antibody information shown in Supplementary Information 1, Table S1) against FKBP5, Ki67, and phospho-P65 (p-P65); washed; incubated with corresponding secondary antibodies; subjected to color development, re-staining, differentiation, dehydration, and blocking steps; and incubated under a microscope (BX53, Olympus. Japan) for observation and recording.

Quantitative real-time reverse transcription PCR (qPCR)

Briefly, the total RNA of the samples was extracted with TRIzol (15596026, Thermo Fisher Scientific Inc.), and the total RNA was reverse transcribed and subjected to qPCR using qPCR kits (RR820A, Takara, Shiga, Japan) in PCR instrument. β-Actin was used as the reference for normalization. The primer information is shown in Supplementary Information 1, Table S2.

Western blotting

The total proteins of the samples were extracted by radioimmunoprecipitation assay (RIPA) (R0010, Solarbio). Protein samples were separated using sodium dodecyl sulfate–polyacrylamide gel electrophoresis, and then the separated proteins were transferred to polyvinylidene fluoride membranes, which were blocked, washed and immersed in primary antibodies against FKBP5, β-actin, cadherin 4 (CDH4), BOK, C-X-C motif chemokine receptor 3 (CXCR3), P65, p-P65, Janus kinase 2 (JAK2), phospho-JAK2 (p-JAK2), signal transducer and activator of transcription 1 (STAT1), and phospho-STAT1 (p-STAT1) (antibody information is shown in Supplementary Information 1, Table S1) and incubated for 12 h. The membranes were rewashed, soaked in secondary antibodies, and incubated for 1 h. The final exposure was performed on an Odyssey infrared imaging system (LI-COR, USA). ImageJ software was used to calculate the grayscale values of the proteins, and β-actin was used as a reference for normalization.

Immunofluorescence

The routine steps of washing, fixation, permeabilization, and blocking were performed for cell samples. The samples were incubated for 12 h in primary antibodies against FKBP5, CD68, and CD86 (antibody information is shown in Supplementary Information 1, Table S1). After rewashing and permeabilization, the samples were incubated in the corresponding secondary antibodies for 30 min. After washing, sealed slices were immediately observed and recorded under fluorescence microscopy.

For wax blocks of tissue samples, after the usual steps of sectioning, dewaxing, antigen retrieval, and blocking, primary antibodies against BOK, CDH4, F4/80, and CD86 were added dropwise, and the sections were incubated overnight. After washing, the corresponding secondary antibodies were added. The samples were incubated with or without tyramide signal amplification reagent. The slices were sealed after restaining with 4′,6-diamidino-2-phenylindole (DAPI). The cells were observed and recorded immediately under a fluorescence microscope.

RNA-sequencing (RNA-seq)

The total RNA of the samples was extracted with an RNAmini Kit (Qiagen, Germany). mRNA enrichment, fragmentation, reverse transcription, library construction, Illumina NovaSeq 6000, and data analysis were performed by Genergy Biotechnology (Shanghai, China).

Cell adhesion ability assay

Fibronectin (F8180, Solarbio) was preincubated in cell culture plates for 1 h, 1% bovine serum albumin after heat denaturation and the plates were washed using basal medium. Cells were grown in culture plates and incubated for 4 h. The unadhered cells were removed by washing with phosphate buffered saline (PBS), and then the number of cells (absorbance values) was calculated using a Cell Counting Kit-8 (CCK-8) kit (CA1210, Solarbio). Finally, the cell adhesion

capacity was calculated (absorbance value of adhered cells over total cells).

Cell–crystal adhesion

After removing the waste medium, the cell samples were added 1 ml of Hanks' Balanced Salt Solution (HBSS), placed on a shaker for 2 min at 150 rpm, shaken four times. Then, HBSS was added again. The samples were immediately observed under an inverted microscope and recorded. Finally, the residual area of crystals was calculated using ImageJ software (ImageJ 1.53s, USA).

Cell viability

A CCK-8 kit was used to detect cell viability. After cell treatment, the waste medium was removed, add the configured CCK-8 working solution was added, and the cells were incubated for 1 h. Finally, the absorbance value of the sample at 450 nm was detected using a microplate reader. Cell viability was calculated according to the absorbance value of the assay wells over the absorbance value of the control wells (the absorbance value of the blank control was be removed).

5-Ethynyl-2′-deoxyuridine (EdU) staining

An EdU kit (C0071S, Beyotime, Shanghai, China) was used to detect the proliferative capacity of cells. EdU working solution was added to the postintervention cell samples and incubated for 2 h, and the waste solution was removed. After washing, fixation, and permeabilization, the configured Click reaction solution was added, and the cells were incubated for 30 min. After washing again and DAPI restaining, the cells were observed and recorded under a fluorescence microscope.

TdT-mediated dUTP nick-end labeling (TUNEL) staining

A TUNEL kit (C1086, Beyotime) was used to detect the apoptosis of cells. Cell samples were washed, fixed, and permeabilized. Tissue samples were sectioned, dewaxed, and incubated with proteinase K for 15 min. Again, the samples were washed well. TUNEL working solution was added, and the samples were incubated for 1 h at 37 °C while protected from light. Immediately after washing again, the cells were recorded under a fluorescence microscope.

Macrophage chemotaxis

M0 macrophages were cultured in the upper chamber, and conditioned medium (CM) was placed in the lower chamber. The CM contained active factors (e.g., chemokines) that induced the movement of M0 macrophages in the upper chamber to the lower chamber. 24 h later, staining was performed using crystal violet. Finally, the cells were observed and recorded under a microscope.

Enzyme-linked immunosorbent assay (ELISA)

An interferon-inducible protein 10 (CXCL10) ELISA Kit (CSB-E08181h/CSB-E08183m, Cusabio, Wuhan, China), and a kidney injury molecule 1 (KIM-1) ELISA Kit (CSB-E08809m, Cusabio) were used to measure CXCL10 and KIM-1, respectively. Incubation of the sample or the mixture of standards and reagents was performed according to the instructions. Finally, the absorbance value of the sample at 450 nm was detected using a microplate reader.

Periodic acid-Schiff (PAS) staining and tubular injury scoring

PAS staining was used to assess renal tubular injury. Kidney tissues were sectioned and dewaxed. They were stained by adding periodic acid staining solution for 15 min and washed twice with distilled water. The tissues were incubated for 30 min in Schiffer's staining solution and rinsed under running water for 5 min. After hematoxylin restaining and blocking, the sections were recorded under a microscope. Finally, renal tubular injury was scored according to a previous study [17].

Serum creatinine (CRE) and blood urea nitrogen (BUN)

A CRE assay kit (C011-2-1, njjcbio, Nanjing, China) and a BUN assay kit (C013-2-1, njjcbio) were used to determine CRE and BUN levels in serum samples. Incubation of the samples or the mixture of standards and reagents was performed according to the instructions. Finally, the absorbance values of the samples at 546 nm (CRE) and 640 nm (BUN) were measured using a microplate reader.

Statistical analysis

GraphPad Prism software (GraphPad Software, version 9.0.0, La Jolla, CA, USA) was used for data analysis. Experimental data were obtained from three or more independent experiments and are expressed as the mean ± standard error of the mean (SEM). Student's *t* test was performed to analyze differences between two groups, and one-way ANOVA was used to analyze differences among multiple groups. Pearson's correlation test was used to analyze the correlation between the two factors. $P < 0.05$ was considered to indicate statistical significance.

Results

The abundance of FKBP5 expression was significantly increased in CaOx kidney stones.

To investigate the status of FKBP5 in CaOx kidney stones, it was first necessary to understand its expression pattern in CaOx kidney stones. Gly was used to construct a mouse CaOx kidney stone model, and Von Kossa staining showed significant stone aggregation in the kidneys of mice after Gly intervention (Fig. 1A, B). Next, immunohistochemistry and qPCR results revealed substantial increases in both FKBP5 protein expression (Fig. 1C, D) and mRNA expression (Fig. 1F) in the kidneys of mice after Gly intervention. Furthermore, Pearson's correlation analysis revealed that the amount of stone deposition in the kidneys of mice and their FKBP5 protein expression (Fig. 1E) or mRNA expression (Fig. 1G) were positively correlated. Subsequently, we constructed in vitro kidney stone models using Ox-stimulated HK-2 cells and HEK-293 cells. The results of Western blotting and qPCR experiments confirmed that Ox stimulation of HK-2 cells and HEK-293 cells upregulated the protein expression (Fig. 1H–J) and mRNA expression (Fig. S1A, B) of FKBP5. Moreover, it was noteworthy that the most significant increase in FKBP5 expression was observed at 36 h of Ox treatment. Therefore, we used immunofluorescence to monitor the fluorescence intensity of FKBP5 after 36 h of Ox intervention, as shown in (Fig. 1K, L), and the fluorescence intensity of FKBP5 in HK-2 cells and HEK-293 cells was significantly increased after 36 h of Ox intervention. These data suggested that the abundance of FKBP5 was increased dramatically in the CaOx kidney stone model, which provided a foundation for a possible important role and position of FKBP5 in CaOx kidney stones.

FKBP5 deficiency inhibits the adhesion capacity and cell–crystal adhesion of RTEC

To continue investigating the role and mechanism of FKBP5 in CaOx kidney stones, RNA-seq was used to analyze the genetic changes of FKBP5 deficiency in HK-2 cells after Ox intervention. As shown in Fig. 2A, with criteria of a |log2 fold change (FC)| ≥ 1 and a false discovery rate (FDR) ≤ 0.05, there were 104 downregulated genes, 134 upregulated genes, and 35,943 non-differentially expressed genes. Kyoto Encyclopedia of Genes and Genomes (KEGG) analysis (Fig. 2B) showed that the cell adhesion molecules were the most significantly enriched pathway. Cell–crystal adhesion has been reported to be essential for forming CaOx kidney stones [3]. Therefore, we knocked down and overexpressed *FKBP5* in HK-2 cells and HEK-293 cells (Fig. S2A, B). Then we measured the cell adhesion ability and cell–crystal adhesion status after *FKBP5* overexpression or knockdown. The cell adhesion ability assay results revealed that Ox intervention increased the adhesion ability of HK-2 cells (Fig. 2C) and HEK-293 cells (Fig. 2D), and *FKBP5* overexpression exacerbated this change. At the same time, *FKBP5* knockdown significantly attenuated this change. Similarly, the results of cell–crystal adhesion assays showed that *FKBP5* overexpression increased the adhesion between HK-2 cells (Fig. 2E, F) and HEK-293 cells (Fig. 2E, G) and Ox crystals, while *FKBP5* knockdown did the opposite. The Heatmap (Fig. 2H) shows the differentially expressed genes enriched in the cell adhesion molecule signaling pathway. We observed that CDH4 was significantly downregulated after the knockdown of *FKBP5*. CDH4 is a classic cell adhesion molecule closely associated with cell adhesion behavior [18]. It has been reported that CDH4 mRNA is significantly increased in the urine of patients with CaOx kidney stones [19]. For this reason, we hypothesized that FKBP5 may influence cell adhesion behavior by regulating the transcription of CDH4. The results of qPCR (Fig. 2I, J) and Western blotting (Fig. 2K–M) revealed that Ox causes upregulation of the mRNA and protein expression of CDH4 in HK-2 cells and HEK-293 cells, and that overexpression of *FKBP5* exacerbates CDH4 upregulation, while knockdown of *FKBP5* inhibits it. Next, we overexpressed *CDH4* in HK-2 and HEK-293 cells and continued examining their cell adhesion behavior. The cell adhesion capacity (Fig. 2N, O) and cell–crystal adhesion (Fig. 2P–R) results showed that overexpression of *CDH4* significantly reversed the cell–crystal adhesion and cell adhesion capacity attenuated by *FKBP5* knockdown. These results confirm that FKBP5 deficiency in RTEC attenuates cell–crystal adhesion and inhibits cell adhesion capacity, and that this effect may be mediated by modulation of CDH4.

FKBP5 deficiency inhibits Ox-induced apoptosis and promotes the proliferation of RTEC

Apoptosis is known to be an essential biological process in the formation of CaOx kidney stones [20, 21]. KEGG analysis showed that the apoptosis-multiple species signaling pathway was similarly enriched (Fig. 3A). Therefore, we examined cell survival, proliferation, and apoptosis. CCK-8 (Fig. 3B) and EdU staining (Fig. 3C–E, Fig. S2D) results showed that Ox inhibited cell viability and cell proliferation in HK-2 cells and HEK-293 cells, and that overexpression of *FKBP5* exacerbated this inhibition, which was alleviated by knockdown of *FKBP5*. TUNEL staining (Fig. 3F–H) showed that Ox increased apoptosis in HK-2 cells and HEK-293 cells, that overexpression of *FKBP5*

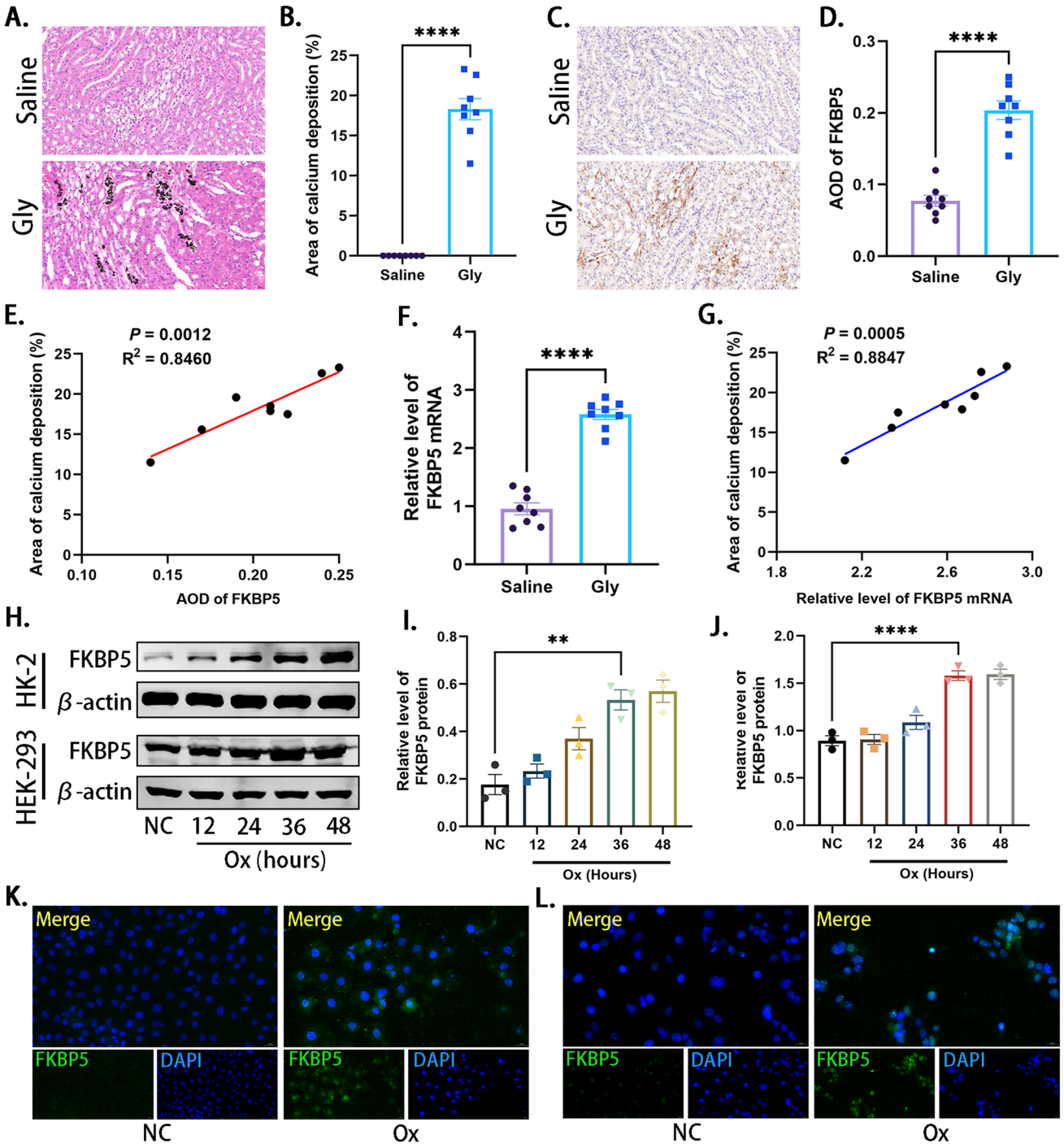

Fig. 1 The abundance of FKBP5 expression was significantly increased in CaOx kidney stones. **A**, **B** Representative images (**A**) and quantitative plots (**B**) of Von Kossa staining showing the extent of calcium salt deposition in the kidneys of mice in the saline and glyoxylate groups. **C**, **D** Representative images (**C**) and quantitative plots (**D**) of immunohistochemistry showing the amount of FKBP5 expression in the kidneys of mice. **E** Pearson correlation analysis of the amount of calcium salt deposition and protein expression of FKBP5. **F** qPCR showing the mRNA expression of FKBP5 relative to β-actin in mouse kidneys. **G** Pearson correlation analysis of the amount of calcium salt deposition and mRNA expression of FKBP5. **H**–**J** Representative images (**H**) and quantitative plots (**I**, **J**) of Western blotting showing the protein expression of FKBP5 in HK-2 cells and HEK-293 cells relative to that of β-actin. **K**, **L** Immunofluorescence images of HK-2 cells (**K**) and HEK-293 cells (**L**) showing FKBP5 expression in the normal control (NC) and Ox groups. All data are expressed as mean ± SEM. Each data point of animal experiments **A**–**G** represents one mouse. Each data point of cell experiments **H**–**L** represents one independent experiment. $^{**}P < 0.01$, $^{****}P < 0.0001$

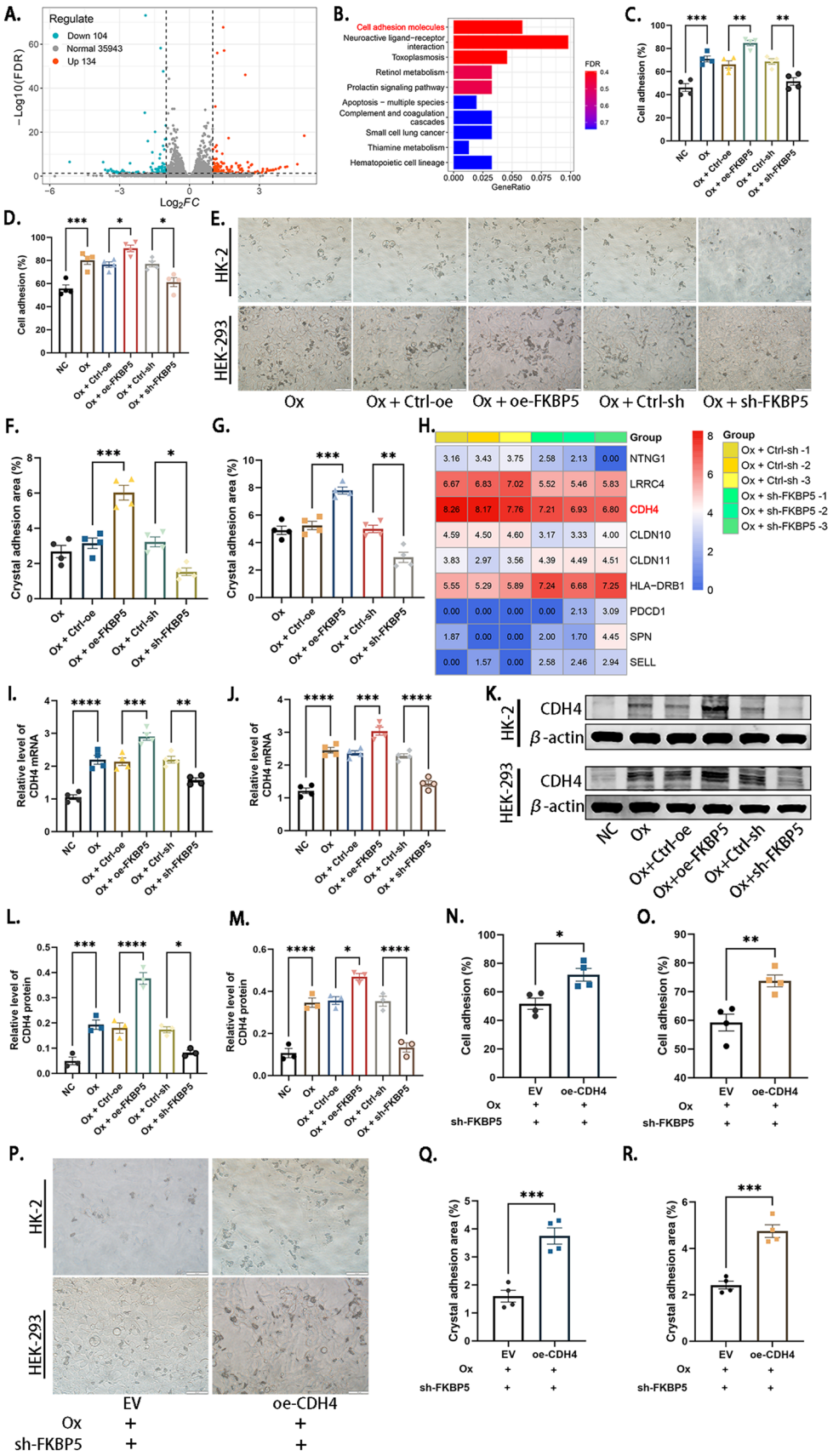

Fig. 2 FKBP5 deficiency inhibits the adhesion capacity and cell–crystal adhesion of RTEC. **A** The volcano plot is from RNA-seq performed on the Ox + FKBP5 knockout (sh-FKBP5) group and the Ox + viral negative control (Ctrl-sh) group, which shows differential gene expression in the Ox + sh-FKBP5 group compared to the Ox + Ctrl-sh group, where gray dots represent genes with no significant difference, red dots indicate upregulated differentially regulated genes, and blue dots indicate downregulated differentially regulated genes. **B** KEGG histogram showing the functional annotations of the differentially expressed genes in **A**. **C**, **D** The cell adhesion ability of HK-2 cells (**C**) and HEK-293 cells (**D**). **E**–**G** Representative images (**E**) and quantitative plots (**F**, **G**) of cell–crystal adhesion of HK-2 cells and HEK-293 cells. **H** Heatmap showing the differentially expressed genes enriched in the cell adhesion molecules in **B**. **I**, **J** qPCR showing the mRNA expression of CDH4 relative to β-actin in HK-2 cells (**I**) and HEK-293 cells (**J**). **K**–**M** Western blot images (**K**) and quantitative plots (**L**, **M**) of CDH4 relative to β-actin in HK-2 cells and HEK-293 cells. **N**, **O** Cell adhesion ability of HK-2 cells (**N**) and HEK-293 cells (**O**). **P**–**R** Representative images (**P**) and quantitative plots (**Q**, **R**) of cell–crystal adhesion of HK-2 cells and HEK-293 cells. All data are expressed as mean ± SEM. Each data point of cellular experiments **A**–**R** represents one independent experiment. $^{*}P < 0.05$, $^{**}P < 0.01$, $^{***}P < 0.001$ and $^{****}P < 0.0001$

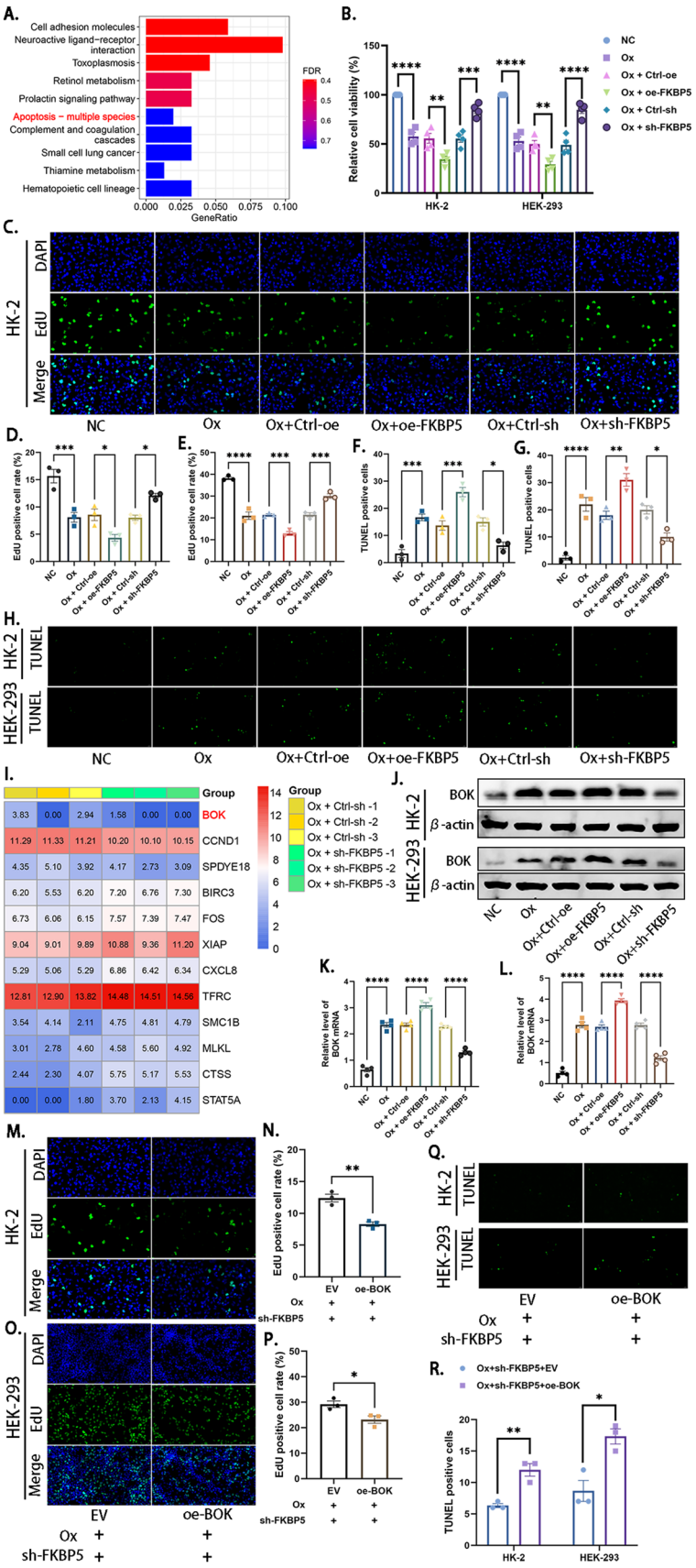

Fig. 3 FKBP5 deficiency inhibits Ox-induced apoptosis and promotes the proliferation of RTEC. **A** KEGG histogram showing the functional annotations of the differential expressed genes in Fig. 2A. **B** CCK-8 assay for cell viability of HK-2 cells and HEK-293 cells. **C**–**E** Representative images (**C**) and quantitative plots (**D**, **E**) of EdU staining to detect the proliferative capacity of HK-2 cells and HEK-293 cells. **F**–**H** Quantitative plots (**F**, **G**) and representative images (**H**) of the extent of apoptosis detected in HK-2 cells and HEK-293 cells by TUNEL staining. **I** Heatmap showing the differentially expressed genes enriched in apoptosis-multiple species of **A**. **J** Western blotting images (K) of BOK protein expression in HK-2 cells and HEK-293 cells. **K**, **L** qPCR showing the mRNA expression of BOK relative to β-actin in HK-2 cells (**K**) and HEK-293 cells (**L**). **M**–**P** Representative images (**M**, **O**) and quantitative plots (**N**, **P**) of EdU staining to detect the proliferative capacity of HK-2 cells and HEK-293 cells. **Q**, **R** Representative images (**Q**) and quantitative plots (**R**) of the extent of apoptosis detected in HK-2 cells and HEK-293 cells by TUNEL staining. All data are expressed as mean ± SEM. Each data point of cellular experiments **A**–**R** represents one independent experiment. *$P < 0.05$, **$P < 0.01$, ***$P < 0.001$ and ****$P < 0.0001$

further enhanced apoptosis, and that knockdown of *FKBP5* alleviated apoptosis. The differentially expressed genes enriched in the apoptosis-multiple species signaling pathways are presented in the formation of heatmap (Fig. 3I). We found that BOK was the most significantly differentially expressed gene. BOK has been reported to induce apoptosis by mediating mitochondrial outer membrane permeabilization [22]. Next, Western blotting (Fig. 3J, Fig. S2E, G) and qPCR (Fig. 3K, L) results revealed that Ox upregulated BOK expression in HK-2 cells and HEK-293 cells and that overexpression of *FKBP5* further enhanced BOK upregulation. In contrast, knockdown of *FKBP5* inhibited BOK upregulation. To continue investigating whether BOK plays an essential role in the effects of FKBP5 deficiency on proliferation and apoptosis in CaOx kidney stone models, we overexpressed BOK in HK-2 and HEK-293 cells. CCK-8 (Fig. S2F, H) and EdU staining (Fig. 3M–P) showed that BOK overexpression reversed the cell viability and proliferation enhanced by FKBP5 deficiency. TUNEL staining (Fig. 3Q, R) showed that overexpression of *BOK* reversed the apoptosis inhibited by FKBP5 deficiency. These data suggest that FKBP5 deficiency protects against Ox-mediated apoptosis in RTEC and promotes their proliferation. Moreover, this protective effect is exerted through inhibition of BOK expression.

FKBP5 deficiency in RTEC inhibits macrophage chemotaxis and M1 polarization

Gene Ontology (GO) analysis revealed that FKBP5 deficiency in RTEC is closely related to the regulation of cytokine biosynthetic process, cytokine biosynthetic processes, cytokine metabolic process, regulation of multicellular organismal process, chemotaxis, and multicellular organismal process (Fig. 4A). It is well known that macrophages act as essential actors in forming CaOx kidney stones. Kidney stones are associated with the presence of M1 macrophages (pro-inflammatory) and the suppression of M2 macrophages (anti-inflammatory) [23]. Therefore, we hypothesized that FKBP5 deficiency in RTEC would affect macrophage behavior through cytokines or chemokines. We intervened in THP-1-induced M0 macrophages using CM of RTEC and assayed the chemotaxis and polarization status of macrophages. The qPCR results showed that the CM of HK-2 cells (Fig. 4B) and HEK-293 cells (Fig. 4C) after Ox treatment significantly promoted the expression of markers of M1 polarization (CD86, TNF-α, and IL-12) and inhibited the expression of markers of M2 polarization (CD206, IL-10, and CD163) in macrophages. Moreover, *FKBP5* overexpression in HK-2 cells and HEK-293 cells enhanced M1 polarization, while *FKBP5* knockdown reversed M1 polarization. Similarly, dual immunofluorescence (Fig. 4D, Fig. S3A) results of CD68 and CD86 confirmed this effect. Next, the macrophage chemotaxis assay results indicated that the CM of HK-2 cells (Fig. 4E, Fig. S3C) and HEK-293 cells (Fig. S3B, D) after Ox treatment significantly promoted macrophage chemotaxis. Moreover, *FKBP5* overexpression in HK-2 cells and HEK-293 cells further enhanced macrophage chemotaxis, whereas *FKBP5* knockdown inhibited macrophage chemotaxis. We next investigated what factors in CM mediate the exchange of FKBP5 deficiency in RTEC with the polarization and chemotaxis of macrophages. We display the functionally annotated differentially expressed genes enriched in GO analysis highlighted in red in the heatmap (Fig. 4F). Among the chemokines were CXCL13, CXCL10, CXCL17, and CXCL8, which were then validated using qPCR, which showed that CXCL10 was the chemokine with the most pronounced expression difference after *FKBP5* knockdown in HK-2 cells (Fig. 4G) and HEK-293 cells (Fig. 4H). Next, ELISA results showed that Ox increased CXCL10 levels in the CM of HK-2 cells (Fig. 4I) and HEK-293 cells (Fig. 4J) and that *FKBP5* overexpression further increased CXCL10 levels, while *FKBP5* knockdown did the opposite. CXCR3 is a receptor for CXCL10 [24]. Western blotting showed that CM of HK-2 cells (Fig. 4K, Fig. S3E) and HEK-293 cells (Fig. 4K, Fig. S3F) after Ox treatment promoted CXCR3 expression in macrophages and that *FKBP5* knockdown in HK-2 cells and HEK-293 cells inhibited this promotion. Then, to further verify the effect of CXCL10, additional CXCL10 was added to the CM, and the polarization and chemotaxis status of macrophages were examined. qPCR (Fig. 4L, M) and immunofluorescence (Fig. 4N, O) showed that CXCL10 addition reversed M1 polarization inhibited by FKBP5 deficiency in RTEC. Macrophage chemotaxis assay results (Fig. 4P, Fig. S3G, H) showed that CXCL10 addition reversed chemotaxis inhibited by FKBP5 deficiency in RTEC. The above data confirm that FKBP5 deficiency in RTEC downregulates CXCL10 expression, which inhibits M1 polarization and chemotaxis of macrophages.

The obstruction of NF-κB signaling is crucial for the inhibition of cell–crystal adhesion, apoptosis, and macrophage M1 polarization and chemotaxis by FKBP5 deficiency in RTEC

It has been reported that FKBP5 is an essential regulator of NF-κB signaling [5]. Thus, to investigate the signaling pathway through which FKBP5 exerts the above effect, we measured the activation of NF-κB signaling in HK-2 cells and HEK-293 cells. Western blotting (Fig. 5A, B) showed that *FKBP5* overexpression enhanced P65 phosphorylation in HK-2 cells and HKK-293 cells, whereas *FKBP5* knockdown inhibited P65 phosphorylation. Next, NF-κB activator 1 was used as an activator of NF-κB signaling to further detect cell proliferation, apoptosis, cell–crystal adhesion of RTEC, and polarization status of macrophages. CCK-8

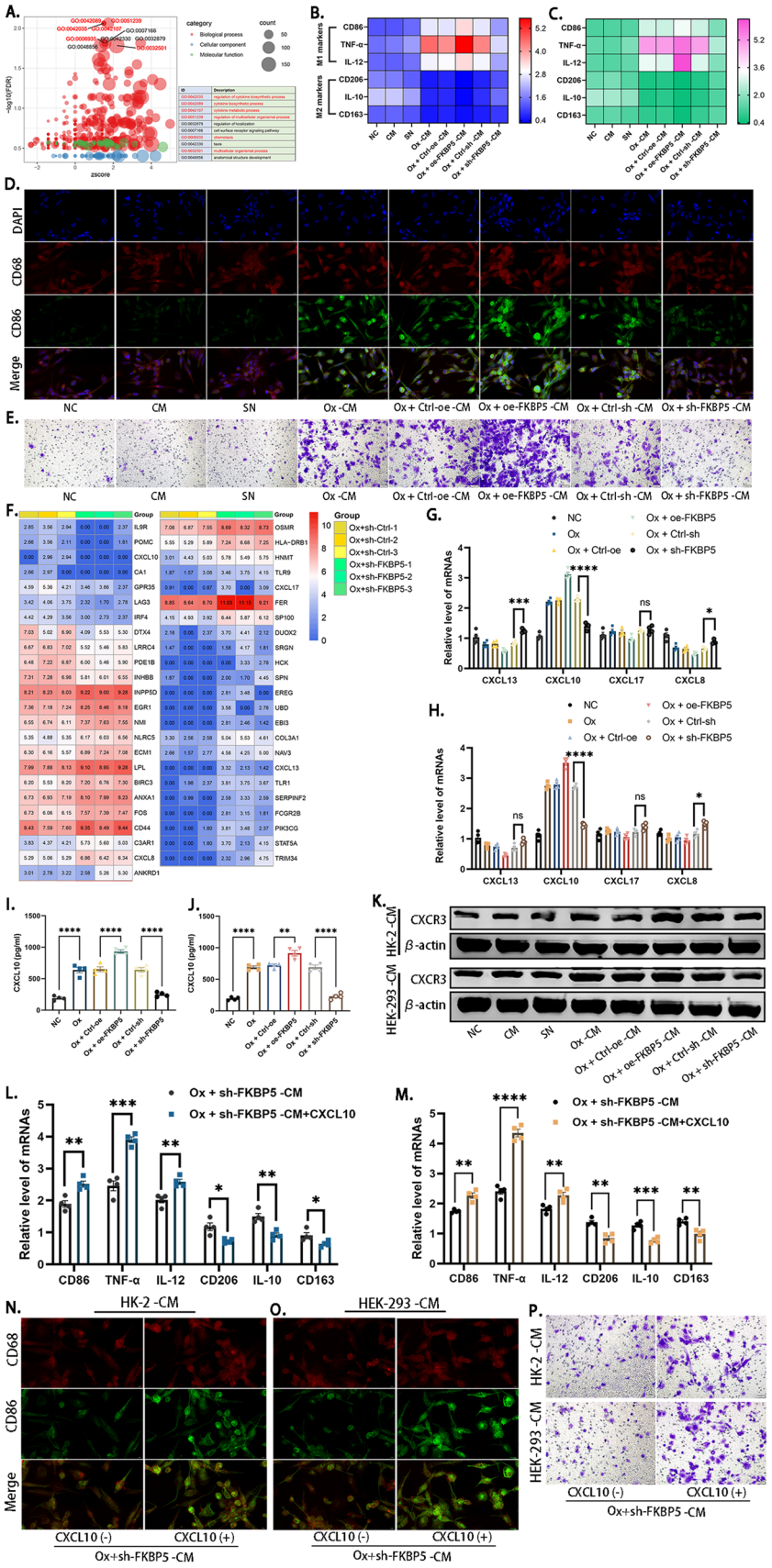
A.
B.
C.
D.
DAPI
CD68
CD86
Merge
NC
CM
SN
Ox -CM
Ox + Ctrl-oe -CM
Ox + oe-FKBP5 -CM
Ox + Ctrl-sh -CM
Ox + sh-FKBP5 -CM
E.
F.
G.
Relative level of mRNAs
CXCL13
CXCL10
CXCL17
CXCL8
H.
I.
J.
CXCL10 (pg/ml)
K.
CXCR3
β-actin
HK-2 -CM
HEK-293 -CM
L.
Ox + sh-FKBP5 -CM
Ox + sh-FKBP5 -CM+CXCL10
CD86
TNF-α
IL-12
CD206
IL-10
CD163
M.
N.
O.
P.
CXCL10 (-)
CXCL10 (+)
Ox+sh-FKBP5 -CM

◂**Fig. 4** FKBP5 deficiency in RTEC inhibits macrophage chemotaxis and M1 polarization. **A** GO bubble diagram showing the functional annotations of the differentially expressed genes in Fig. 2A. **B**, **C** qPCR assay of mRNA expression of M1 macrophage markers (CD86, IL-6, IL-12) and M2 macrophage markers (CD206, IL-10, CD163) relative to β-actin in macrophages after intervention with CM in HK-2 cells (**B**) or HEK-293 cells (**C**). **D** Representative images of dual immunofluorescence detection of CD68 (red) and CD86 (green) expression in macrophages after intervention with CM in HK-2 cells. **E** Representative images of chemotaxis assays detecting macrophages after intervention with CM from HK-2 cells. **F** Heatmap showing the differentially expressed genes enriched in **A** for regulation of cytokine biosynthetic process, cytokine biosynthetic process, cytokine metabolic process, regulation of the multicellular organismal process, chemotaxis, and multicellular organismal process. **G**, **H** qPCR showing the mRNA expression of CXCL13, CXCL10, CXCL17, and CXCL8 relative to β-actin in HK-2 cells (**G**) and HEK-293 cells (**H**). **I**, **J** ELISA assays for the CXCL10 in CM of HK-2 cells (**I**) and HEK-293 cells (**J**). **K** Western blot images of CXCR3 protein expression in macrophages subjected to intervention with CM in HK-2 cells and HEK-293 cells. **L**, **M** qPCR assay of mRNA expression of M1 macrophage markers (CD86, IL-6, IL-12) and M2 macrophage markers (CD206, IL-10, CD163) relative to β-actin in macrophages after intervention with CM in HK-2 cells (**L**) or HEK-293 cells (**M**). **N**, **O** Representative images of dual immunofluorescence detection of CD68 (red) and CD86 (green) expression in macrophages after intervention with CM in HK-2 cells (**N**) and HEK-293 cells (**O**). **P** Representative images of chemotaxis assays detecting macrophages after intervention with CM from HK-2 cells and HEK-293 cells. *NC* normal control, *CM* conditioned medium from HK-2 cells or HEK-293 cells without Ox, *SN* supernatant of Ox, *Ox –CM* conditioned medium from HK-2 cells or HEK-293 cells with Ox. All data are expressed as mean ± SEM. Each data point of cellular experiments in **A**–**P** represents one independent experiment. $^{*}P < 0.05$, $^{**}P < 0.01$, $^{***}P < 0.001$ and $^{****}P < 0.0001$

results (Fig. 5C) and EdU staining (Fig. 5D–F) showed that NF-κB activator 1 reversed the proliferation capacity promotion mediated by FKBP5 deficiency in HK-2 cells and HEK-293 cells. TUNEL staining (Fig. 5G, H) showed that NF-κB activator 1 reversed the apoptosis inhibition mediated by FKBP5 deficiency in HK-2 cells and HEK-293 cells. The results of the cell adhesion capacity assay (Fig. 5I) and crystal adhesion assay (Fig. 5J, K) showed that NF-κB activator 1 reversed the cell adhesion capacity and cell–crystal adhesion inhibition mediated by FKBP5 deficiency in HK-2 cells and HEK-293 cells. Moreover, the qPCR results (Fig. 5L, M) and double immunofluorescence assay (Fig. 5N, O) results showed that NF-κB activator 1 reversed the M1 polarization of macrophages inhibited by FKBP5 deficiency in HK-2 cells and HEK-293 cells. The macrophage chemotaxis assay results (Fig. 5P, Q) showed that NF-κB activator 1 reversed macrophage chemotaxis inhibited by FKBP5 deficiency in HK-2 cells and HEK-293 cells. Then, we further validated the changes in CDH4, BOK, and CXCL10, which are critical targets of FKBP5 deficiency. It was found that NF-κB activator 1 reversed the expression of CXCL10 (Fig. 5R), BOK (Fig. 5S, T), and CDH4 (Fig. 5S, U), which were downregulated by FKBP5 deficiency in HK-2 cells and HEK-293 cells. These experimental results suggest that NF-κB signaling is probably critical for the inhibition of cell–crystal adhesion, apoptosis, macrophage M1 polarization, and chemotaxis caused by FKBP5 deficiency in RTEC.

FKBP5 deficiency in RTEC inhibits the activation of JAK2/STAT1 signaling in macrophages

Subsequently, we attempted to explain what signaling pathways in macrophages are affected by FKBP5 deficiency in RTEC that influence macrophage behavior. Previously, we found that RTEC-derived CXCL10 is critical for macrophage polarization. CXCL10 promotes macrophage M1 polarization by activating JAK2/STAT1 signaling in macrophages [25]. Therefore, we examined the activation of JAK2/STAT1 signaling in macrophages after intervention with CM. Western blotting results showed that CM from HK-2 cells (Fig. 6A–C) and HEK-293 cells (Fig. 6D–F) with Ox and *FKBP5* overexpression promoted the phosphorylation of JAK2 and STAT1 in macrophages, whereas *FKBP5* knockdown inhibited the phosphorylation of JAK2 and STAT1 in macrophages. Next, to confirm whether JAK2/STAT1 signaling bridges CXCL10's influence on macrophage polarization, we knocked down *JAK2* in macrophages and then examined the polarization and chemotaxis status of macrophages. The qPCR results (Fig. 6G, H) and double immunofluorescence (Fig. 6I) revealed that the knockdown of *JAK2* in macrophages reversed the M1 polarization of macrophages promoted by adding CXCL10. Moreover, macrophage chemotaxis assay results (Fig. 6J) showed that the knockdown of *JAK2* in macrophages also reversed CXCL10 addition-promoted macrophage chemotaxis. These data suggest that FKBP5 deficiency in RTEC reduces CXCL10 secretion, which inhibits the activation of JAK2/STAT1 signaling in macrophages and ultimately inhibits M1 polarization and chemotaxis of macrophages.

FKBP5 deficiency alleviates stone aggregation, kidney injury, and inflammatory macrophage accumulation in CaOx kidney stone mice

In vivo experimental validation is necessary to clearly understand the role and mechanism of FKBP5 in CaOx kidney stones. Therefore, we established CaOx kidney stone mice with Gly and then inhibited FKBP5 expression in the kidneys of the mice with AAV-sh-FKBP5. The results of Von Kossa staining (Fig. 7A, C) and PAS staining (Fig. 7B, D) showed that Gly significantly increased stone aggregation and tubular injury in the kidneys of mice, respectively. In contrast, FKBP5 deficiency alleviated stone aggregation and tubular injury. CRE and BUN, urinary KIM-1 are common indicators of kidney injury [26, 27]. Thus, as shown in Fig. 7E–G, FKBP5 deficiency significantly alleviated

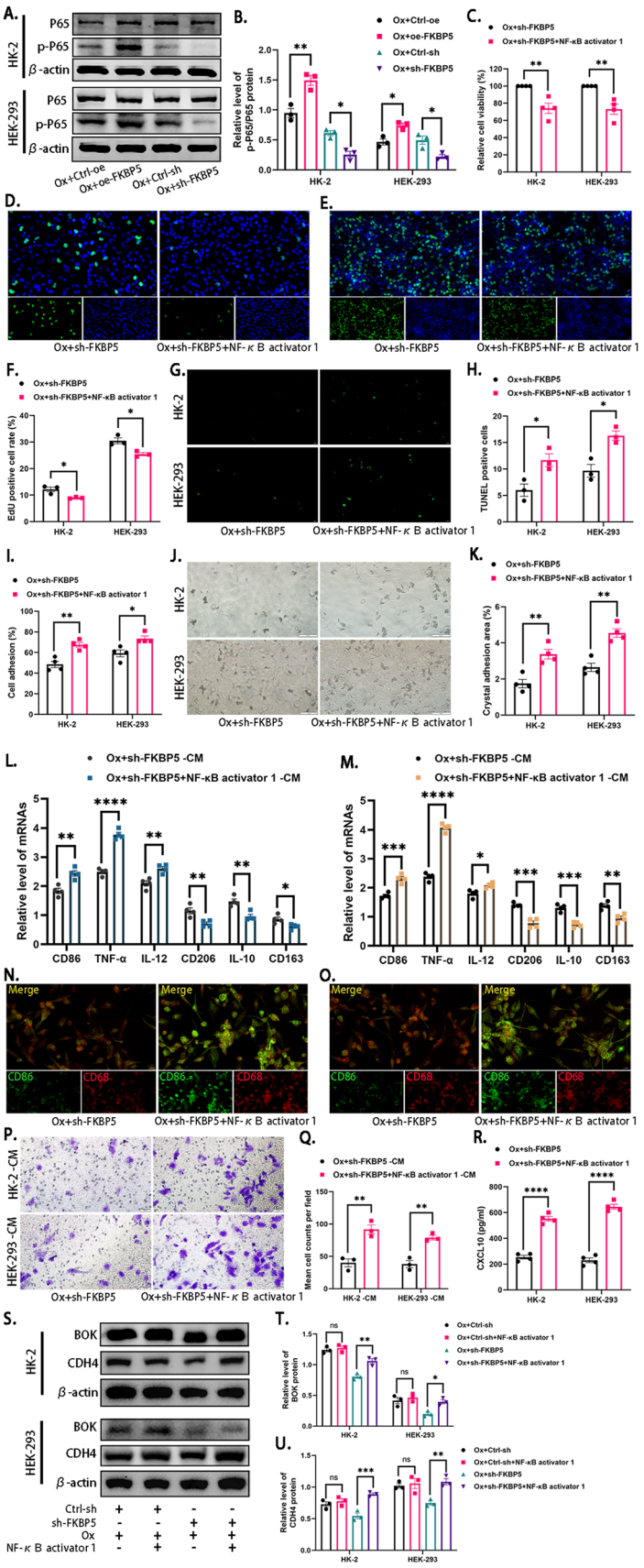
A.
P65
p-P65
β-actin
HK-2
HEK-293
Ox+Ctrl-oe
Ox+oe-FKBP5
Ox+Ctrl-sh
Ox+sh-FKBP5
B.
Relative level of p-P65/P65 protein
C.
Relative cell viability (%)
D.
E.
Ox+sh-FKBP5
Ox+sh-FKBP5+NF-κB activator 1
F.
EdU positive cell rate (%)
G.
H.
TUNEL positive cells
I.
Cell adhesion (%)
J.
K.
Crystal adhesion area (%)
L.
Relative level of mRNAs
CD86
TNF-α
IL-12
CD206
IL-10
CD163
Ox+sh-FKBP5 -CM
Ox+sh-FKBP5+NF-κB activator 1 -CM
M.
N.
Merge
CD68
O.
P.
HK-2 -CM
HEK-293 -CM
Q.
Mean cell counts per field
R.
CXCL10 (pg/ml)
S.
BOK
CDH4
Ctrl-sh
sh-FKBP5
Ox
NF-κB activator 1
T.
Relative level of BOK protein
Ox+Ctrl-sh
Ox+Ctrl-sh+NF-κB activator 1
Ox+sh-FKBP5
Ox+sh-FKBP5+NF-κB activator 1
U.
Relative level of CDH4 protein

◂**Fig. 5** The obstruction of NF-κB signaling is crucial for the inhibition of cell–crystal adhesion, apoptosis, macrophage M1 polarization, and chemotaxis caused by FKBP5 deficiency in RTEC. **A**, **B** Western blot images (**A**) and quantitative plots (**B**) of P65 and p-P65 protein expression relative to β-actin expression in HK-2 cells and HEK-293 cells. **C** CCK-8 assay for cell viability of HK-2 cells and HEK-293 cells. **D**–**F** Representative images (**D**, **E**) and quantitative plots (**F**) of EdU staining to detect the proliferative capacity of HK-2 cells and HEK-293 cells. **G**, **H** Representative images (**G**) and quantitative plots (**H**) of the extent of apoptosis detected in HK-2 cells and HEK-293 cells by TUNEL staining. **I** The cell adhesion ability of HK-2 cells and HEK-293 cells. **J**, **K** Representative images (**J**) and quantitative plots (**K**) of cell–crystal adhesion of HK-2 cells and HEK-293 cells. **L**, **M** qPCR assay of mRNA expression of M1 macrophage markers (CD86, IL-6, IL-12) and M2 macrophage markers (CD206, IL-10, CD163) relative to β-actin in macrophages after intervention with CM in HK-2 cells (**L**) or HEK-293 cells (**M**). **N**, **O** Representative images of dual immunofluorescence detection of CD68 (red) and CD86 (green) expression in macrophages after intervention with CM in HK-2 cells (**N**) and HEK-293 cells (**O**). **P**, **Q** Representative images (**P**) and quantitative plots (**Q**) of chemotaxis assays detecting macrophages chemotaxis after intervention with CM from HK-2 cells and HEK-293 cells. **R** ELISA assays for CXCL10 in the CM of HK-2 cells and HEK-293 cells. **S**–**U** Western blot images (**S**) and quantitative plots (**T**, **U**) of BOK and CDH4 relative to β-actin in HK-2 cells and HEK-293 cells. All data are expressed as mean ± SEM. Each data point of cellular experiments **A**–**U** represents one independent experiment. $*P<0.05$, $**P<0.01$, $***P<0.001$ and $****P<0.0001$, *ns* not significant

kidney injury caused by Gly in mice. Moreover, TUNEL staining (Fig. 7H, Fig. S4A) also showed that FKBP5 deficiency significantly reduced Gly-induced apoptosis in RTEC of mice. Ki67 is a classical indicator of cell proliferative capacity [28]. The immunohistochemistry (Fig. 7I, Fig. S4B) results for Ki67 showed that FKBP5 deficiency significantly increased the proliferative capacity of RTEC in CaOx kidney stone mice. It has been reported that NF-κB signaling is activated considerably in RTEC of Gly-induced CaOx kidney stones [29]. Combined with the results of our in vitro experiments, this finding indicates that NF-κB signaling is an essential mediator of the action of FKBP5. As shown in Fig. 7J, Fig. S4C, Gly significantly increased the expression of p-P65 in RTEC of mouse, and FKBP5 deficiency significantly reversed the expression of p-P65. To further verify the mechanism of FKBP5, we further examined the expression of BOK, CDH4, and CXCL10 in the RTEC of mice kidneys. Immunofluorescence, qPCR, and ELISA results showed that FKBP5 deficiency significantly reduced Gly-induced protein and mRNA expression of BOK (Fig. 7K, M, Fig. S4F), CDH4 (Fig. 7L, N, Fig. S4E) and CXCL10 (Fig. 7O, Fig. S4D) in RTEC. F4/80 is a common macrophage marker in mice [30]. The double immunofluorescence results (Fig. 7P) indicated that FKBP5 deficiency significantly reduced Gly-induced inflammatory macrophage infiltration in mouse kidneys. The above results reaffirm the role and mechanism of FKBP5 in CaOx kidney stones. FKBP5 deficiency attenuates Gly-induced stone aggregation, kidney injury, and inflammatory macrophage infiltration in mouse kidneys.

Activation of NF-κB signaling could hamper the therapeutic effect of FKBP5 deficiency on CaOx kidney stones

To further verify that FKBP5 exerts its action by modulating NF-κB signaling, we performed reversal experiments using NF-κB signaling agonists. Von Kossa staining (Fig. 8A, B) showed that NF-κB activator 1 significantly reversed the reduction in stone aggregation in the kidneys of mice caused by FKBP5 deficiency. The results of CRE (Fig. 8C), BUN (Fig. 8D), and KIM-1 (Fig. S5A) analyses showed that NF-κB activator 1 significantly reversed the protective effect of FKBP5 deficiency against kidney injury in mice. Moreover, the results of TUNEL staining (Fig. 8E, Fig. S5B) showed that NF-κB activator 1 significantly reversed the inhibitory effect of FKBP5 deficiency on apoptosis. Immunohistochemical (Fig. 8F, Fig. S5C) assays showed that NF-κB activator 1 significantly reduced the number of Ki67-positive cells. These data suggest that inhibiting NF-κB signaling mediates the protective effect of FKBP5 deficiency on CaOx kidney stone mice.

Discussion

Although the prevalence and recurrence rates of kidney stones are surprisingly high, kidney stones are not taken as seriously as they should be. Most patients experience kidney stones as renal colic caused by stones becoming lodged in the ureter. However, it is dangerous to take the complications of kidney stones lightly, as stones can cause irreversible kidney damage. The mechanism of renal injury in CaOx kidney stones remains elusive, and FKBP5 is a possible causative factor or predictor of renal injury [5, 8]. Here, we found enrichment of FKBP5 in CaOx kidney stones. FKBP5 deficiency attenuated cell adhesion and cell–crystal adhesion of RTEC by inhibiting NF-κB/CDH4 signaling, reduced apoptosis of RTEC by inhibiting NF-κB/BOK signaling and suppressed M1 polarization and infiltration of macrophages by inhibiting NF-κB/CXCL10 signaling. We also found that FKBP5 deficiency prevented Gly-induced stone aggregation and kidney injury in the kidneys of mice.

Upregulation of FKBP5 is associated with nerve injury, acute kidney injury, diabetes, and other inflammation-related diseases [8, 31, 32]. Interestingly, by examining in vitro and in vivo models of CaOx kidney stones, we found that FKBP5 was highly enriched in RTEC of CaOx kidney stones and positively correlated with the degree of stone aggregation in the mouse kidneys.

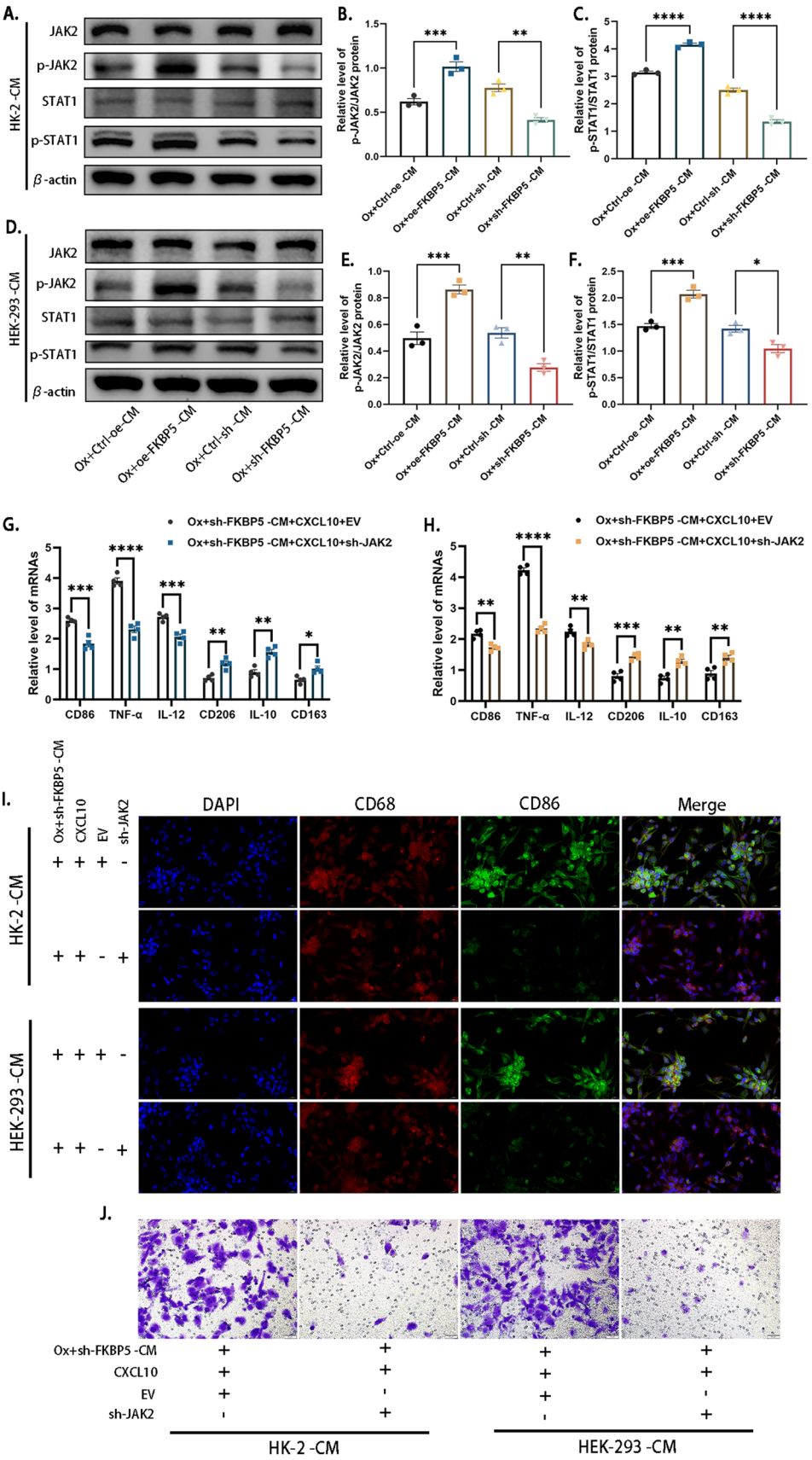

Fig. 6 FKBP5 deficiency in RTEC inhibits the activation of JAK2/STAT1 signaling in macrophages. **A**–**C** Western blotting images (**A**) and quantitative plots (**B**, **C**) of JAK2, p-JAK2, STAT1, and p-STAT1 protein expression relative to β-actin expression in macrophages subjected to intervention with CM in HK-2 cells. **D**–**F** Western blotting images (**D**) and quantitative plots (**E**, **F**) of JAK2, p-JAK2, STAT1, and p-STAT1 protein expression relative to β-actin expression in macrophages subjected to intervention with CM in HEK-293 cells. **G**, **H** qPCR assay of mRNA expression of M1 macrophage markers (CD86, IL-6, IL-12) and M2 macrophage markers (CD206, IL-10, CD163) relative to β-actin in macrophages after intervention with CM in HK-2 cells (**G**) or HEK-293 cells (**H**). **I** Representative images of dual immunofluorescence detection of CD68 (red) and CD86 (green) expression in macrophages after intervention with CM in HK-2 cells and HEK-293 cells. **J** Representative images of chemotaxis assays detecting macrophages after intervention with CM from HK-2 cells and HEK-293 cells. All data are expressed as mean ± SEM. Each data point of cellular experiments **A**–**J** represents one independent experiment. $^{*}P < 0.05$, $^{**}P < 0.01$, $^{***}P < 0.001$ and $^{****}P < 0.0001$

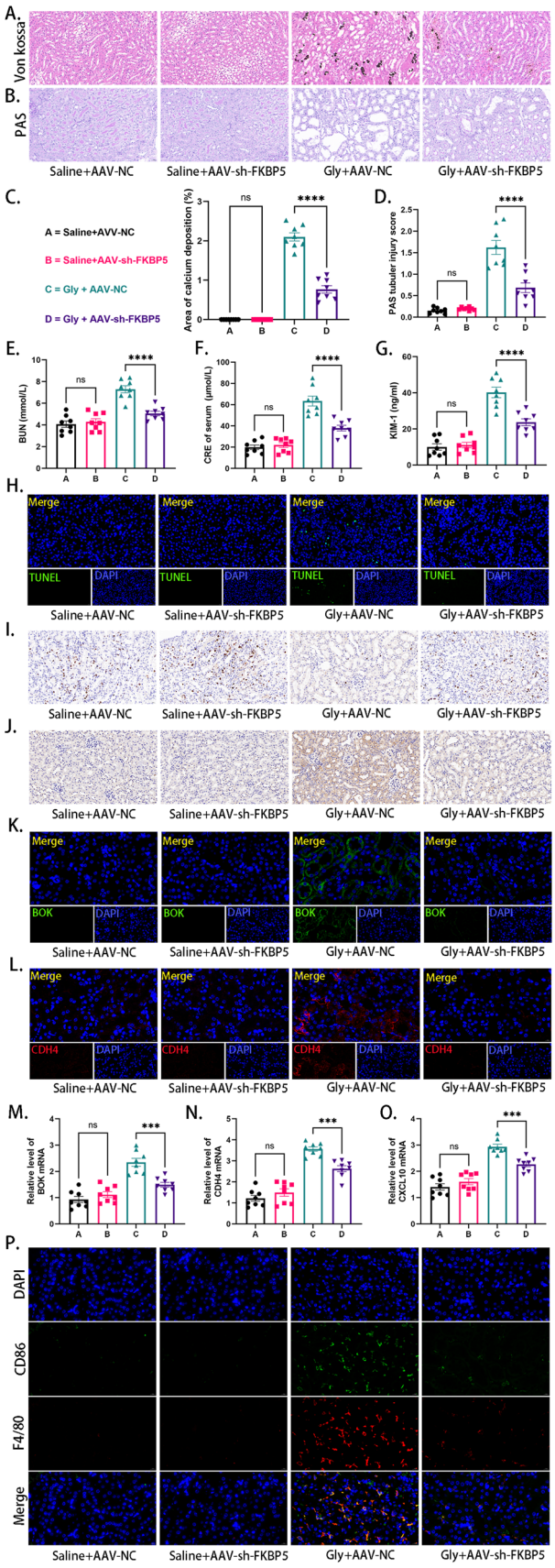

Fig. 7 FKBP5 deficiency alleviates stone aggregation, kidney injury, and inflammatory macrophage accumulation in CaOx kidney stone mice. **A**, **C** Representative images (**A**) and quantitative plots (**C**) of Von Kossa staining showing calcium salt aggregation in mouse kidneys. **B**, **D** Representative images (**B**) and quantitative plots (**D**) of PAS staining showing renal tubular injury in mouse kidneys. **E**, **F** The contents of BUN (**E**) and CRE (**F**) in the serum of each group of mice. **G** Quantitative plots for the detection of KIM-1 in mouse urine by ELISA. **H** Representative images of TUNEL staining to detect tubular epithelial cell apoptosis in mouse kidneys. **I**, **J** Representative images of immunohistochemistry to detect the protein expression of Ki67 (**I**) and p-P65 (**J**) in mouse kidneys. **K**, **L** Representative immunofluorescence images to detect BOK (**K**) and CDH4 (**L**) expression in mouse kidneys. **M**–**O** Quantitative plots of BOK (**M**), CDH4 (**N**), and CXCL10 (**O**) mRNA expression relative to β-actin expression in mouse kidneys by as determined qPCR. **P** Representative images of double immunofluorescence showing the expression of F4/80 (red) and CD86 (green) in the mouse kidneys. All data are expressed as mean ± SEM. Each data point of animal experiments **A**–**P** Represents one mouse. $^{*}P < 0.05$, $^{**}P < 0.01$, $^{***}P < 0.001$ and $^{****}P < 0.0001$, *ns* not significant

In this report, transcriptome sequencing analysis revealed that FKBP5 knockdown resulted in differential expression of genes enriched in the cell adhesion molecule pathway. It has been indicated that cell–crystal adhesion plays an essential role in the overall pathology of CaOx kidney stones [20, 33]. We found that FKBP5 deficiency attenuated cell adhesion capacity and cell–crystal adhesion. Additionally, downregulation of CDH4 was critical for FKBP5 deficiency to exert this effect. This is similar to the findings of previous studies [19, 34], in which the levels of CDH4, a classic cell adhesion molecule, were found to be significantly increased in the urine of patients with CaOx kidney stones.

It is well known that renal tubular epithelial cell apoptosis is involved in the pathogenesis of CaOx kidney stones [35]. Here, we found that FKBP5 deficiency attenuated Ox-induced apoptosis and enhanced cell proliferation via transcriptome sequencing and cell survival assays. We also found that BOK is critical for FKBP5 deficiency to inhibit apoptosis. It was downregulated with the knockdown of FKBP5. BOK has been reported to be an essential apoptosis-inducing molecule [22].

Given the vital role of macrophage polarization, CaOx kidney stones might be considered an immune-related disease [23]. In this study, we found that FKBP5 deficiency was highly associated with cytokine production and multicellular communication. We then examined the role of FKBP5 in the communication between RTEC and macrophage polarization. CXCL10 is a chemokine associated with M1 polarization and chemotaxis of macrophages [36]. We found that FKBP5 deficiency could inhibit macrophage M1 polarization and chemotaxis by downregulating CXCL10 expression. We verified that downregulation of CXCL10 inhibited macrophage polarization by inhibiting JAK2/STAT1 signaling through JAK2 knockdown and reversal experiments

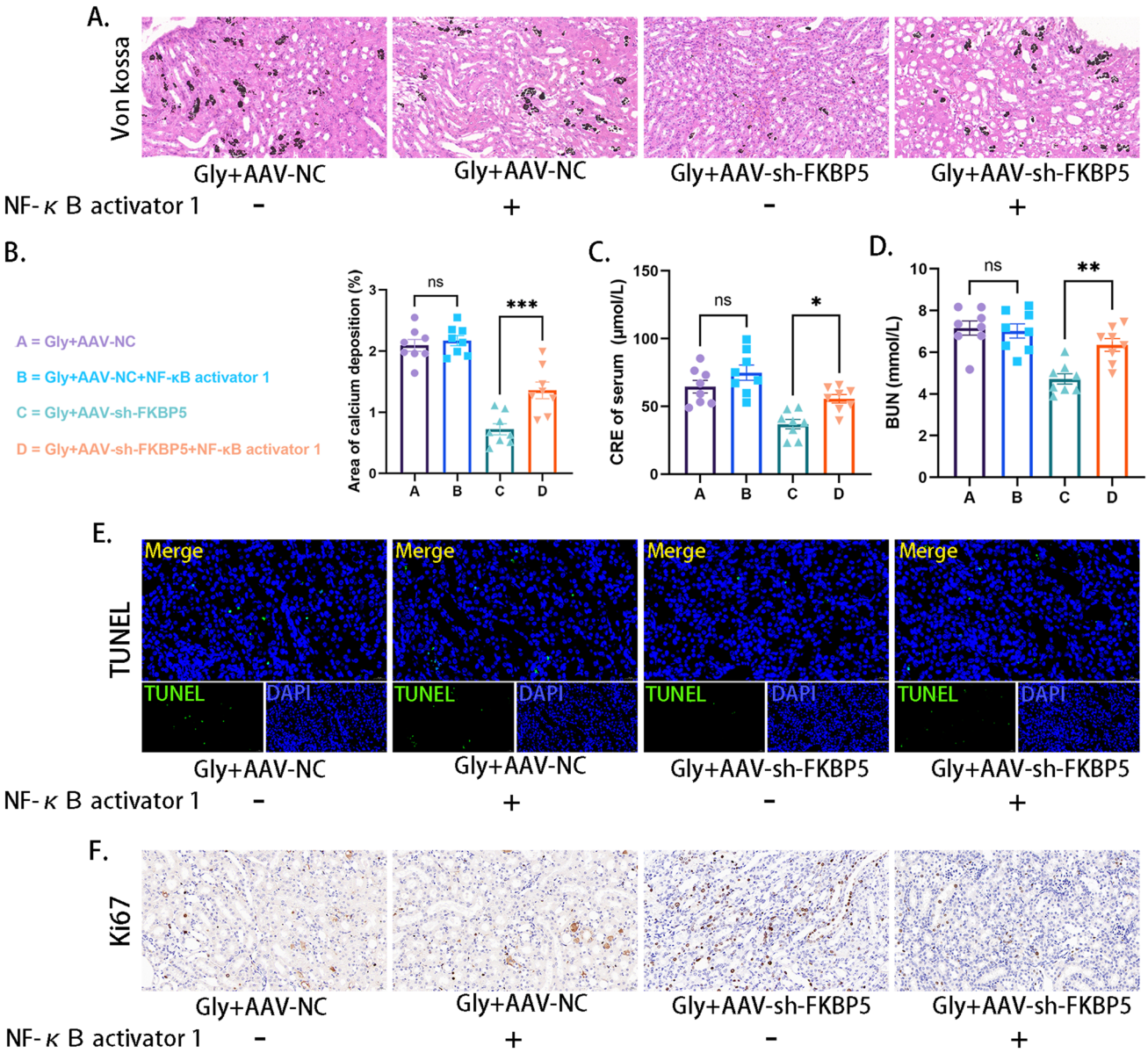

Fig. 8 Activation of NF-κB signaling could hamper the therapeutic effect of FKBP5 deficiency on CaOx kidney stones. **A**, **B** Representative images (**A**) and quantitative plots (**B**) of Von Kossa staining showing calcium salt aggregation in mouse kidneys. **C**, **D** Levels of CRE (**C**) and BUN (**D**) in serum in each group of mice. **E** Representative images of TUNEL staining to detect tubular epithelial cell apoptosis in mouse kidneys. **F** Representative images of immunohistochemistry to detect the protein expression of Ki67 in the mouse kidneys. All data are expressed as mean ± SEM. Each data point of animal experiments **A**–**F** represents one mouse. $^{*}P < 0.05$, $^{**}P < 0.01$, $^{***}P < 0.001$, *ns* not significant

in macrophages. This is consistent with the findings of a previous study [25]. Here, we used only JAK2 knockdown to inhibit the activation of JAK2/STAT1 signaling, so we cannot exclude other STATs, and specific JAK2/STAT1 signaling inhibitors may be needed for further confirmation.

It has been confirmed that NF-κB signaling is a vital pathway for FKBP5 to function [10]. And NF-κB signaling is an essential inflammatory signal for CaOx kidney stones [37]. Here, Western blotting confirmed that phosphorylation of P65 was significantly increased by FKBP5 overexpression, whereas FKBP5 knockdown inhibited P65 phosphorylation. P65 is one of the critical components of NF-κB signaling [38]. We also re-examined cell adhesion, cell–crystal adhesion, cell proliferation, apoptosis, and macrophage polarization. We found that NF-κB signaling is crucial for the role of FKBP5 in CaOx kidney stones, confirming our initial speculation.

Finally, in vivo results further confirmed that FKBP5 deficiency in the kidney attenuated Gly-induced kidney stone aggregation and kidney injury in mice. Moreover, activators of NF-κB signaling were able to reverse the therapeutic effects of FKBP5 deficiency on stone and kidney injury. Unfortunately, since the FKBP5 deficiency and NF-κB activation in mice were not targeted to RTEC, other cells in the kidney (including macrophages) were also affected. Therefore, this study did not entirely exclude a potential effect caused by FKBP5 deficiency or NF-κB signaling agonism in macrophages or other cells.

Conclusion

We demonstrate, for the first time, that FKBP5 deficiency in RTEC can treat stone aggregation and kidney injury in CaOx kidney stones. This therapeutic effect is exerted by inhibition of NF-κB signaling and downregulation of the expression of CDH4, BOK, and CXCL10, which attenuates the adhesion of RTEC to crystals, reduces apoptosis of RTEC, promotes the proliferation of RTEC and inhibits M1 polarization and chemotaxis of macrophages. Based on our findings, FKBP5 may be a promising target for treating or diagnosing CaOx kidney stones.

Supplementary Information The online version contains supplementary material available at https://doi.org/10.1007/s00018-023-04958-7.

Author contributions SXY, LJX, and QLS designed the research and wrote the manuscript; QLS, CS, XC, LJL, and WBL performed the experiments; CS, WBL, and LJX analyzed data; QLS, XC, CS, and YHX performed the animal model, and performed critical reading/editing of the manuscript; SXY and LJX supervised the study.

Funding This work was supported by the National Natural Science Foundation of China (No. 82070723) and (No. 82270797).

Data availability The raw data of RNA-seq were shown in Supplementary Information 2. Other data will be made available on request.

Declarations

Conflict of interest The authors have declared that no conflict of interest exists.

Ethical approval The animal experiments in this study were approved by the Animal Ethics Committee of the Renmin Hospital of Wuhan University (Issue No. 20221008A).

Informed consent Not applicable.

References

1. Zeng G, Mai Z, Xia S et al (2017) Prevalence of kidney stones in China: an ultrasonography based cross-sectional study. BJU Int 120:109
2. Abufaraj M, Xu T, Cao C et al (2021) Prevalence and trends in kidney stone among adults in the USA: analyses of National Health and Nutrition Examination Survey 2007–2018 Data. Eur Urol Focus 7:1468
3. Khan SR, Pearle MS, Robertson WG et al (2016) Kidney stones. Nat Rev Dis Primers 2:16008
4. Keddis MT, Rule AD (2013) Nephrolithiasis and loss of kidney function. Curr Opin Nephrol Hypertens 22:390
5. Li L, Lou Z, Wang L (2011) The role of FKBP5 in cancer aetiology and chemoresistance. Br J Cancer 104:19
6. Zannas AS, Jia M, Hafner K et al (2019) Epigenetic upregulation of FKBP5 by aging and stress contributes to NF-kappaB-driven inflammation and cardiovascular risk. Proc Natl Acad Sci USA 116:11370
7. Hartmann J, Bajaj T, Klengel C et al (2021) Mineralocorticoid receptors dampen glucocorticoid receptor sensitivity to stress via regulation of FKBP5. Cell Rep 35:109185
8. Xu H, Wang Z (2022) MicroRNA-23a-3p ameliorates acute kidney injury by targeting FKBP5 and NF-kappaB signaling in sepsis. Cytokine 155:155898
9. Lawrence T (2009) The nuclear factor NF-kappaB pathway in inflammation. Cold Spring Harb Perspect Biol 1:a001651
10. Bouwmeester T, Bauch A, Ruffner H et al (2004) A physical and functional map of the human TNF-alpha/NF-kappa B signal transduction pathway. Nat Cell Biol 6:97
11. Avellino R, Romano S, Parasole R et al (2005) Rapamycin stimulates apoptosis of childhood acute lymphoblastic leukemia cells. Blood 106:1400
12. Liu H, Ye T, Yang X et al (2019) H19 promote calcium oxalate nephrocalcinosis-induced renal tubular epithelial cell injury via a ceRNA pathway. EBioMedicine 50:366
13. Okada A, Nomura S, Higashibata Y et al (2007) Successful formation of calcium oxalate crystal deposition in mouse kidney by intraabdominal glyoxylate injection. Urol Res 35:89
14. Miller AW, Choy D, Penniston KL et al (2019) Inhibition of urinary stone disease by a multi-species bacterial network ensures healthy oxalate homeostasis. Kidney Int 96:180
15. Renkema KY, Lee K, Topala CN et al (2009) TRPV5 gene polymorphisms in renal hypercalciuria. Nephrol Dial Transplant 24:1919
16. Vezzoli G, Terranegra A, Aloia A et al (2013) Decreased transcriptional activity of calcium-sensing receptor gene promoter 1 is associated with calcium nephrolithiasis. J Clin Endocrinol Metab 98:3839
17. Liu H, Yang X, Tang K et al (2020) Sulforaphane elicts dual therapeutic effects on renal inflammatory injury and crystal deposition in calcium oxalate nephrocalcinosis. Theranostics 10:7319
18. Polanco J, Reyes-Vigil F, Weisberg SD et al (2021) Differential spatiotemporal expression of type I and type II cadherins associated with the segmentation of the central nervous system and formation of brain nuclei in the developing mouse. Front Mol Neurosci 14:633719
19. Liang X, Lai Y, Wu W et al (2019) LncRNA–miRNA–mRNA expression variation profile in the urine of calcium oxalate stone patients. BMC Med Genom 12:57
20. Li Y, Lu X, Yu Z et al (2023) Meta-data analysis of kidney stone disease highlights ATP1A1 involvement in renal crystal formation. Redox Biol 61:102648
21. Ding T, Zhao T, Li Y et al (2021) Vitexin exerts protective effects against calcium oxalate crystal-induced kidney pyroptosis in vivo and in vitro. Phytomedicine 86:153562
22. Vandenabeele P, Bultynck G, Savvides SN (2023) Pore-forming proteins as drivers of membrane permeabilization in cell death pathways. Nat Rev Mol Cell Biol 24:312

23. Khan SR, Canales BK, Dominguez-Gutierrez PR (2021) Randall's plaque and calcium oxalate stone formation: role for immunity and inflammation. Nat Rev Nephrol 17:417
24. Tokunaga R, Zhang W, Naseem M et al (2018) CXCL9, CXCL10, CXCL11/CXCR3 axis for immune activation—a target for novel cancer therapy. Cancer Treat Rev 63:40
25. Zhang J, Liu Y, Chen H et al (2022) MyD88 in hepatic stellate cells enhances liver fibrosis via promoting macrophage M1 polarization. Cell Death Dis 13:411
26. Chen Y, Li C, Duan S et al (2019) Curcumin attenuates potassium oxonate-induced hyperuricemia and kidney inflammation in mice. Biomed Pharmacother 118:109195
27. Schrezenmeier EV, Barasch J, Budde K et al (2017) Biomarkers in acute kidney injury—pathophysiological basis and clinical performance. Acta Physiol (Oxf) 219:554
28. Miller I, Min M, Yang C et al (2018) Ki67 is a graded rather than a binary marker of proliferation versus quiescence. Cell Rep 24:1105
29. Ming S, Tian J, Ma K et al (2022) Oxalate-induced apoptosis through ERS-ROS-NF-kappaB signalling pathway in renal tubular epithelial cell. Mol Med 28:88
30. van den Berg TK, Kraal G (2005) A function for the macrophage F4/80 molecule in tolerance induction. Trends Immunol 26:506
31. Yu S, Yu M, Bu Z et al (2020) FKBP5 exacerbates impairments in cerebral ischemic stroke by inducing autophagy via the AKT/FOXO3 pathway. Front Cell Neurosci 14:193
32. Sidibeh CO, Pereira MJ, Abalo XM et al (2018) FKBP5 expression in human adipose tissue: potential role in glucose and lipid metabolism, adipogenesis and type 2 diabetes. Endocrine 62:116
33. Sheng X, Jung T, Wesson JA et al (2005) Adhesion at calcium oxalate crystal surfaces and the effect of urinary constituents. Proc Natl Acad Sci USA 102:267
34. Ceresa D, Alessandrini F, Bosio L et al (2019) Cdh4 down-regulation impairs in vivo infiltration and malignancy in patients derived glioblastoma cells. Int J Mol Sci 20:4028
35. Abhishek A, Benita S, Kumari M et al (2017) Molecular analysis of oxalate-induced endoplasmic reticulum stress mediated apoptosis in the pathogenesis of kidney stone disease. J Physiol Biochem 73:561
36. Liang T, Chen J, Xu G et al (2022) STAT1 and CXCL10 involve in M1 macrophage polarization that may affect osteolysis and bone remodeling in extrapulmonary tuberculosis. Gene 809:146040
37. Tozawa K, Yasui T, Okada A et al (2008) NF-kappaB activation in renal tubular epithelial cells by oxalate stimulation. Int J Urol 15:924
38. Chen T, Wang Y, Xu Z et al (2019) Epstein–Barr virus tegument protein BGLF2 inhibits NF-kappaB activity by preventing p65 Ser536 phosphorylation. FASEB J 33:10563